# Supplementary Information

## Structural basis for assembly and function of the *Salmonella* flagellar MS-ring with three different symmetries

**Miki Kinoshita, Fumiaki Makino, Tomoko Miyata, Katsumi Imada, Keiichi Namba, Tohru Minamino**

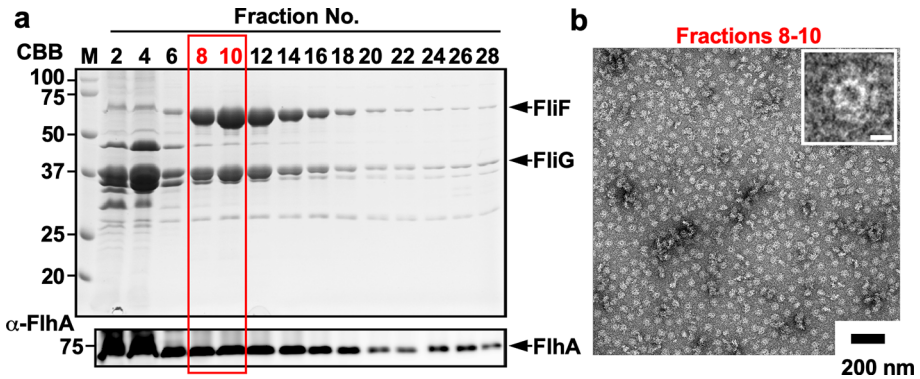


**Supplementary Fig. 1. Co-purification of the MS-ring with FliG and FlhA by sucrose gradient ultracentrifugation. (a)** SDS-PAGE band pattern of each fraction after sucrose gradient ultracentrifugation. After SDS-PAGE, proteins in each fraction were analyzed by Coomassie Brilliant blue staining and immunoblotting with polyclonal anti-FlhA antibody (α-FlhA). The positions of molecular mass markers (kDa) are shown on the left. The regions of interest were cropped from original gel images shown in Supplementary Fig. 16. **(b)** Negative stained EM image of purified MS-rings. Fractions 8, 9, and 10 containing FliF, FliG, and FlhA were collected and concentrated by ultracentrifugation. Concentrated samples were negatively stained with 2% (w/v) uranyl acetate and observed by electron microscopy. Electron micrographs were recorded at a magnification of x20,000. The inset indicates a magnified view of the MS-ring. Scale bar shown in inset, 10 nm.

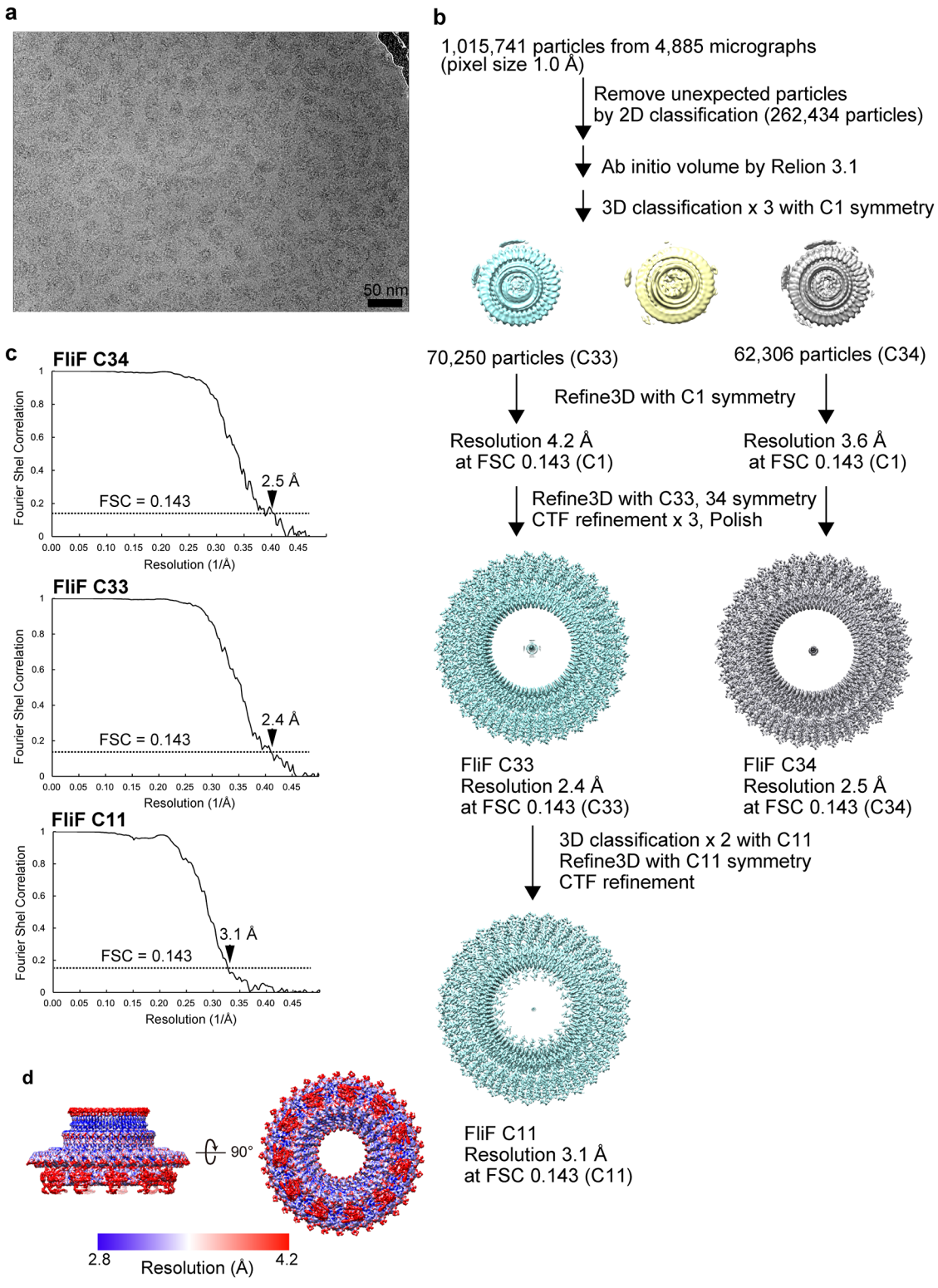


**Supplementary Fig. 2. CryoEM single particle 3D image analysis of the MS-ring.** **(a)** Representative cryoEM image of the MS-rings formed by co-expression of FliF with FliG and transmembrane export gate proteins. **(b)** Work process of cryoEM single particle 3D reconstruction. **(c)** Fourier shell correlation (FSC) curve of the final density map of the FliF-ring reconstructed with C34 (EMDB ID: EMD-60009) (upper), C33 (EMDB ID: EMD-60008) (middle), or C11 (EMDB ID: EMD-60007) (lower) symmetry

applied. **(d)** Local resolution of the final density map of the FliF-ring with C11 symmetry applied is colored from blue (2.8 Å) to red (4.2 Å).

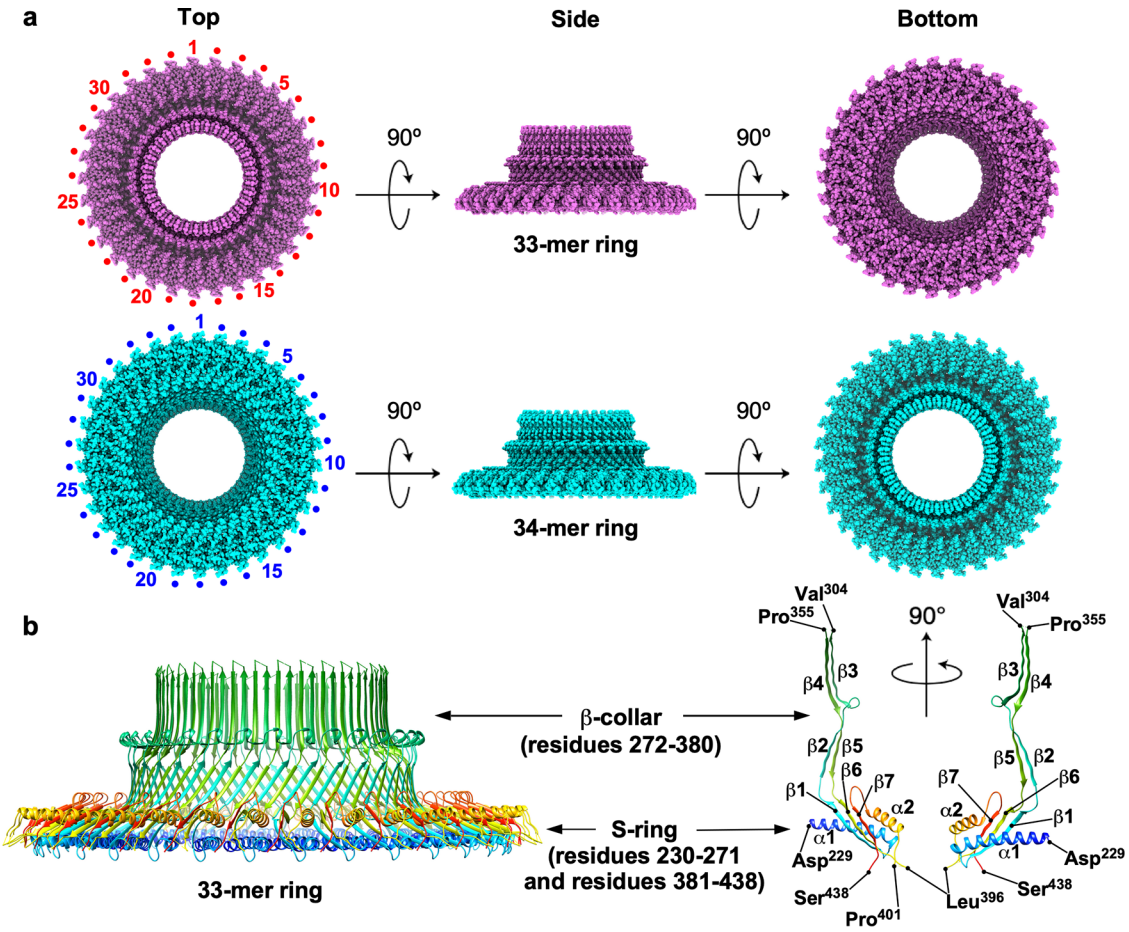


**Supplementary Fig. 3. The RBM3-ring structures. (a)** CryoEM structures of the 33-mer and 34-mer RBM3-rings with C33 (PDB ID: 8ZDT) (upper) and C34 (PDB ID: 8ZDU) (lower) symmetry applied, respectively. **(b)** Cα ribbon diagrams of the RBM3-ring with C33 symmetry applied (left) and the RBM3 subunit forming the S-ring and β-collar (right). The Cα backbone is color-coded from blue to red, going through the rainbow colors from the N-terminus to the C-terminus.

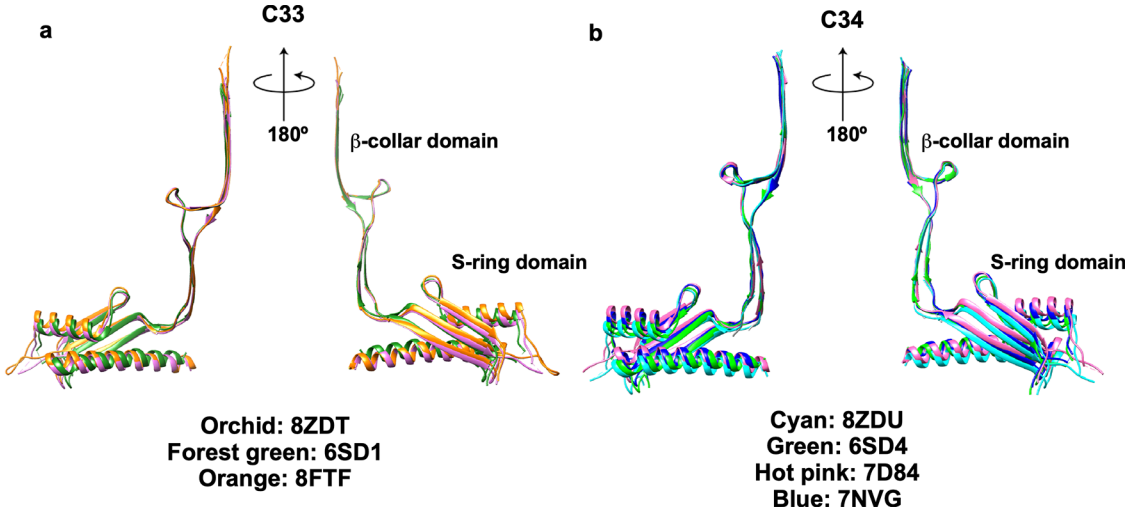


**Supplementary Fig. 4. Structural comparison of various *Salmonella* FliF subunits. (a)** The 33-mer RBM3-ring. The β-collar domains of the FliF subunit of the 6SD1 (forest green) and 8FTF (orange) ring structures were superimposed on the corresponding domain of the coordinates obtained in this study (PDB ID: 8ZDT). **(b)** The 34-mer RBM3-ring. The β-collar domains of the FliF subunit of the 6SD4 (green), 7D84 (hot pink), and 7NVG (blue) ring structures were superimposed on the equivalent domain of the coordinates obtained in this study (PDB ID: 8ZDU).

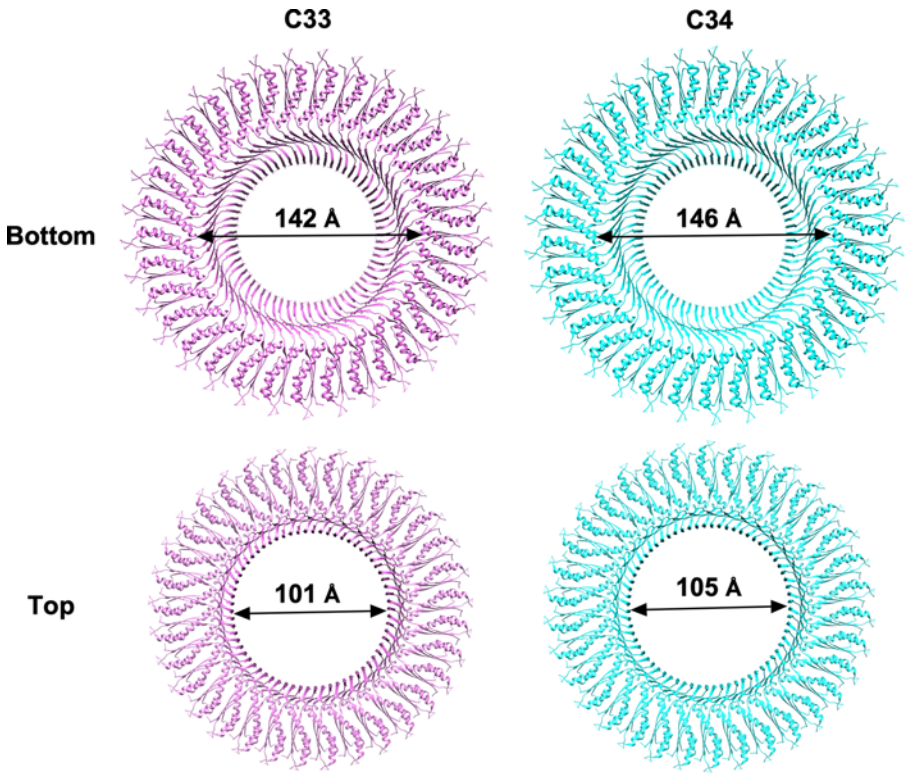


**Supplementary Fig. 5. Inner diameters of the 33-mer (PDB ID: 8ZDT) (left panels) and C34-mer (PDB ID: 8ZDU) (right panels) RBM3-rings.** The distance between Asp-229 of Mol-A and Asp-229 of Mol-Q and that between Asp-229 of Mol-A and Asp-229 of Mol-R were measured as the inner diameter of the 33-mer and 34-mer S-ring, respectively (upper panels). The distance between Pro-355 of Mol-A and Pro-355 of Mol-Q and that between Pro-355 of Mol-A and Pro-355 of Mol-R were measured as the inner diameter of the 33-mer and 34-mer β-collar, respectively (lower panels).

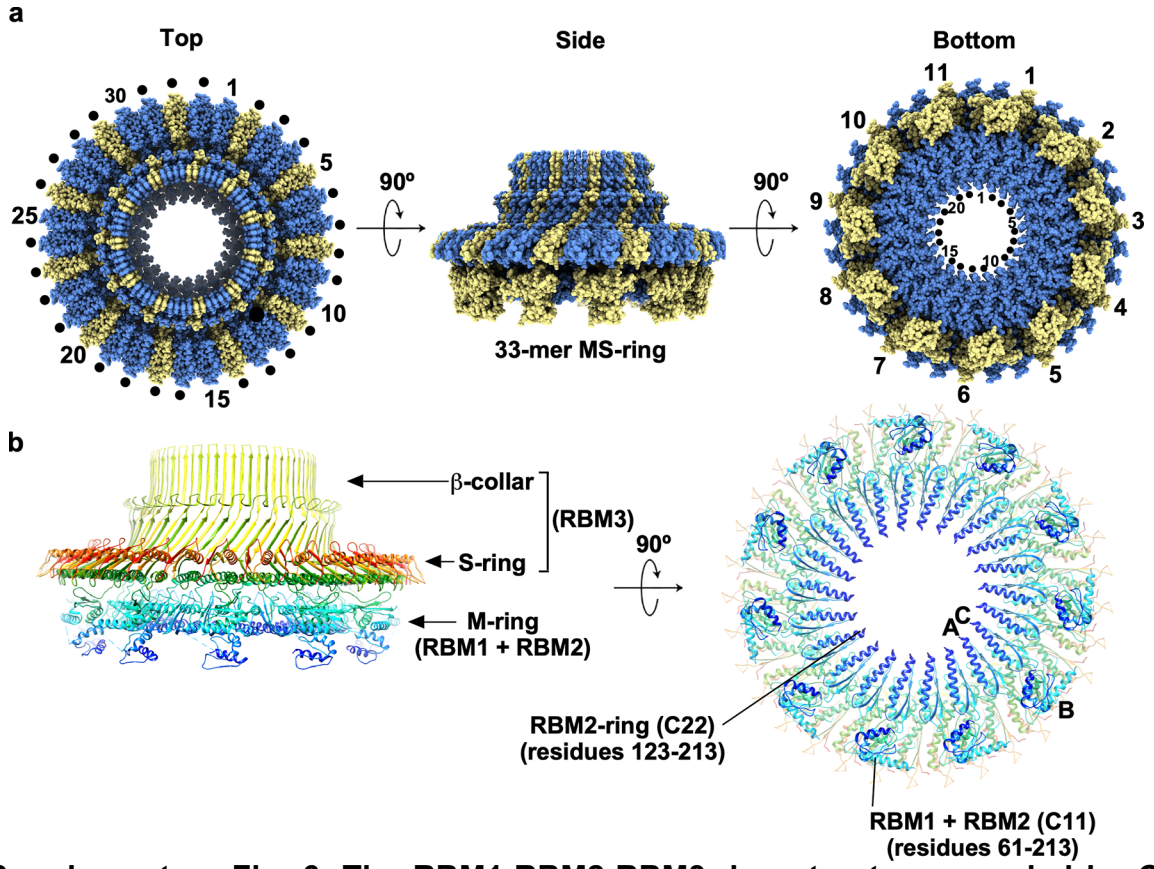


**Supplementary Fig. 6. The RBM1-RBM2-RBM3-ring structure revealed by C11 symmetry enforcement. (a)** CryoEM structure of the 33-mer MS-ring with C11 symmetry applied (PDB ID: 8ZDS). All 33 RBM3 domains form the 33-mer S-ring and β-collar, while 22 RBM2 domains face inward to form the inner core ring of the M-ring, and the remaining 11 RBM2 domains form cog-like structures with 11 RBM1 domains on the outer surface of the inner core ring. The densities for the remaining 22 RBM1 domains, presumably located below the 22-mer inner core RBM2-ring, are not observed clearly. FliF subunits are colored either cornflower blue or khaki to identify the two different conformations: cornflower blue for its RBM2 forming the 22-mer inner core ring; and khaki for its RBM2 forming the cog-like structure. **(b)** Cα ribbon diagrams of the atomic model. The Cα backbone is color-coded from blue to red, going through the rainbow colors from the N-terminus to the C-terminus. RBM2 (residues 123–213) forms the 22-mer RBM2-ring as well as the 11 cog-like structures with RBM1 (residues 61–113) just outside the RBM2-ring.

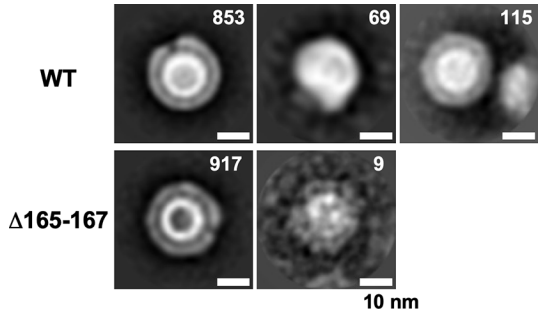


**Supplementary Fig. 7. Representative 2D class average images of the MS-ring formed by wild-type FliF (upper panels) or FliF(Δ165-167) (lower panels).** Reference-free 2D class average images were calculated by RELION 4.0.0. All scale bars indicate 10 nm. The number of particles for each class is indicated in the top right corner.

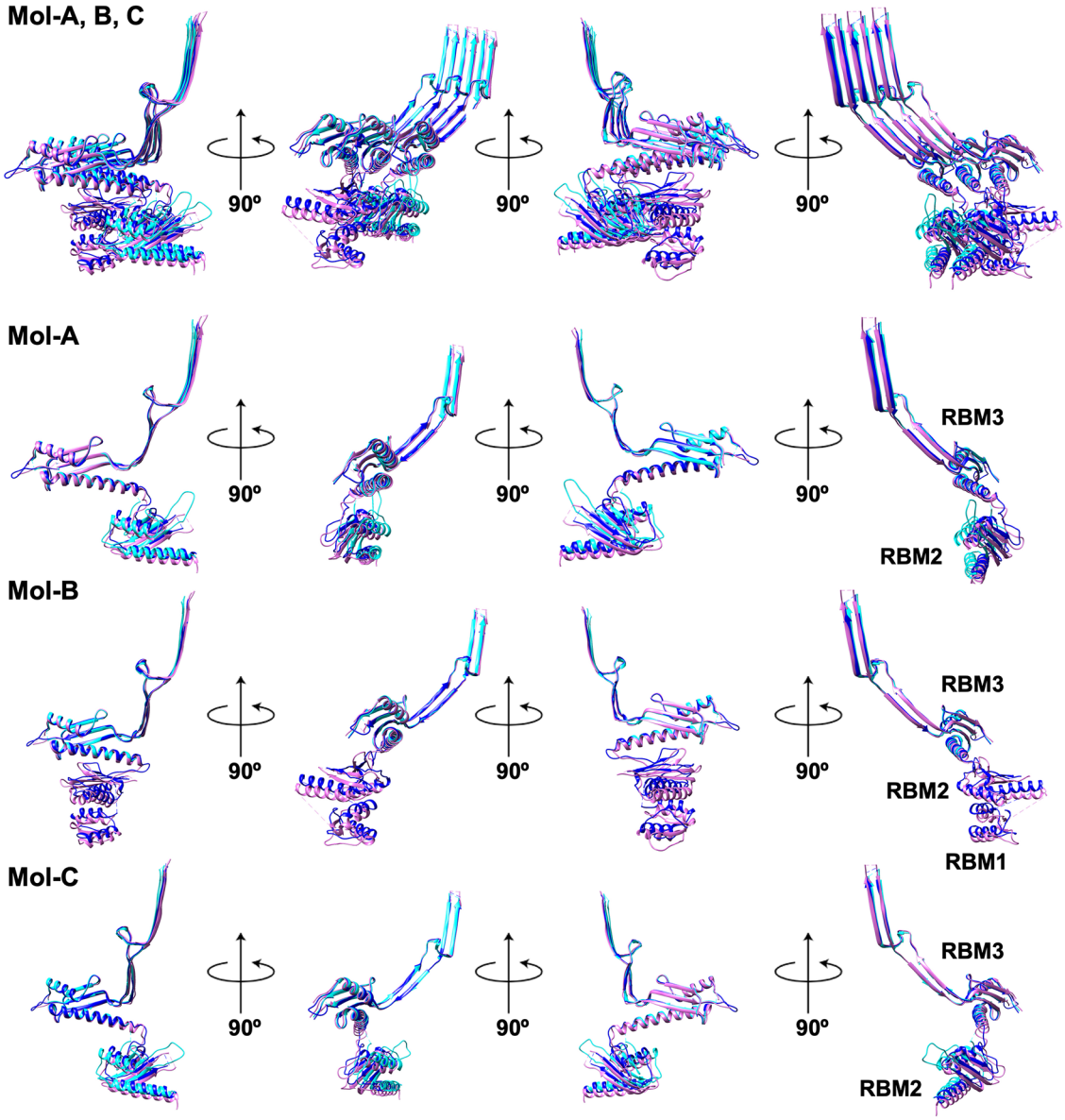


**Orchid, 8ZDS; Blue, 8T8P; Cyan, 7NVG**

**Supplementary Fig. 8. Superposition of three FliF subunits obtained in this study (PDB ID: 8ZDS) (orchid) with equivalent coordinate regions of the 8T8P (blue) and 7NVG (cyan) structures.** The β-collar domain of one of the FliF subunits of the 8T8P (blue) or 7NVG (cyan) ring was superimposed on the corresponding domain of Mol-A of the MS-ring obtained in this study to compare the structure of three subunits together as well as the conformation of each subunit.

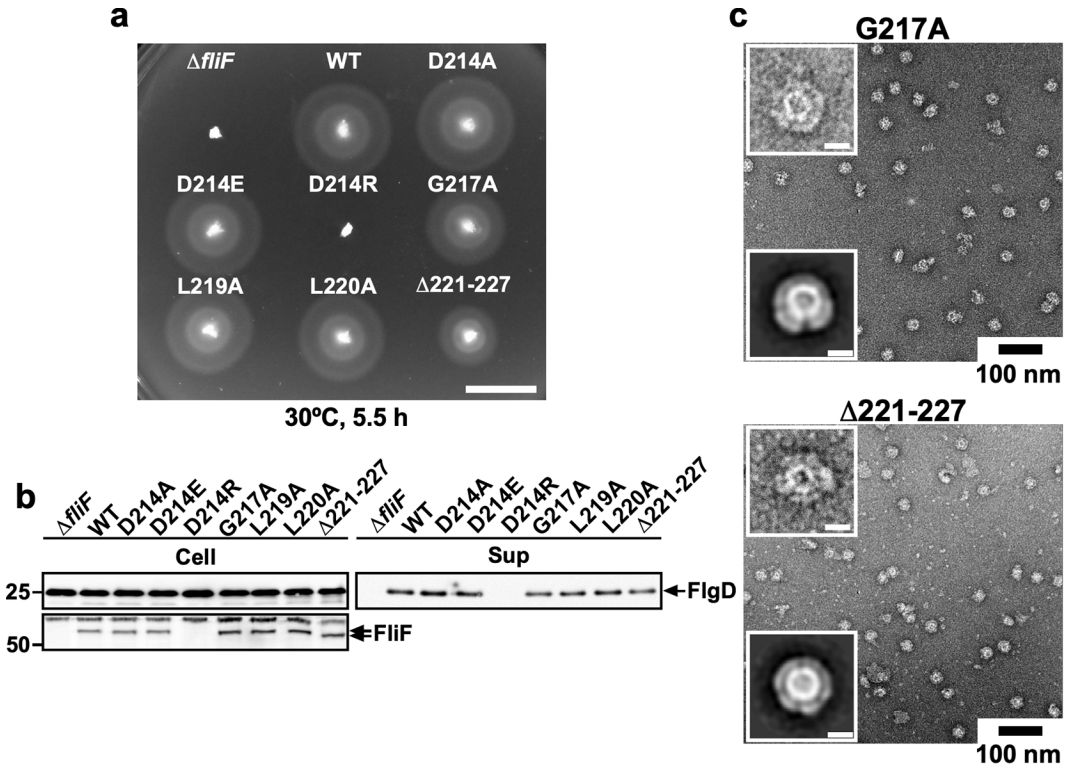


**Supplementary Fig. 9. Mutational analysis of the RBM2-3 loop connecting RBM2 and RBM3. (a)** Motility of a *Salmonella fliF* null mutant harboring pTrc99AFF4 (indicated as △*fliF*), pMKMiF015 (indicated as WT), pMKMiF015(D214A) (indicated as D214A), pMKMiF015(D214E) (indicated as D214E), pMKMiF015(D214R) (indicated as D214R), pMKMiF015(G217A) (indicated as G217A), pMKMiF015(L219A) (indicated as L219A), pMKMiF015(L220A) (indicated as L220A), or pMKMiF015(Δ221–227) (indicated as Δ221–227) in soft agar. The plate was incubated at 30ºC for 5.5 hours. Scale bar, 1.0 cm. At least seven independent measurements were performed. **(b)** Secretion assays. Whole cell proteins (Cell) and culture supernatant fractions (Sup) were prepared from the above transformants. A 5 μl solution of each protein sample, which was normalized to an optical density of $OD_{600}$, was subjected to SDS-PAGE, followed by immunoblotting with polyclonal anti-FlgD (first row) or anti-FliF (second row) antibody. The positions of molecular mass markers (kDa) are shown on the left. The regions of interest were cropped from original immunoblots shown in Supplementary Fig. 17. At least three independent assays were carried out. **(c)** Negative stained EM images of the MS-rings isolated from the G217A and Δ221–227 mutants. Electron micrographs were recorded at a magnification of x50,000. Upper and lower insets indicate enlarged views of the MS-ring and representative 2D class average images calculated by RELION 4.0.0 (See Supplementary 10). Scale bars shown in insets, 10 nm. Independent sample preparations were carried out at least three times.

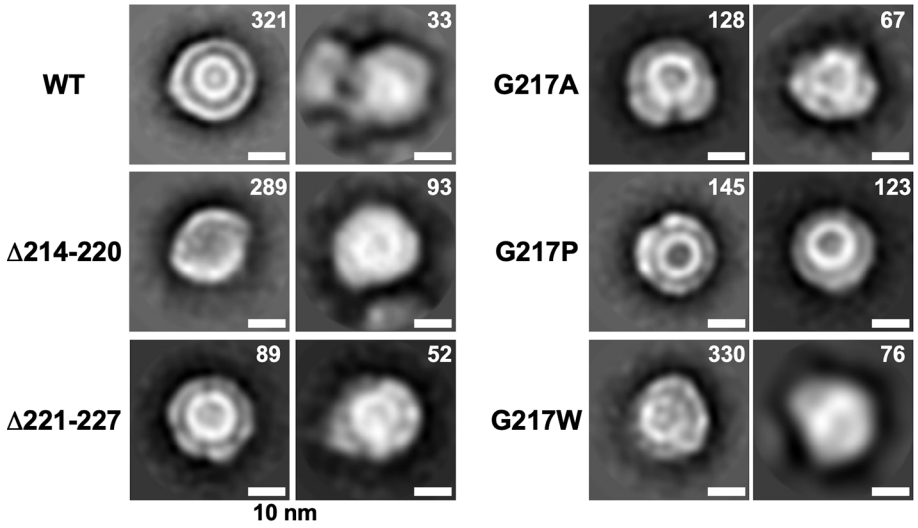


**Supplementary Fig. 10. Effect of various mutations in the RBM2-3 loop on MS-ring formation.** Reference-free 2D class average images were calculated by RELION 4.0.0. Two major classes are shown for the wild-type and mutant strains. All scale bars indicate 10 nm. The number of particles for each class is indicated in the top right corner.

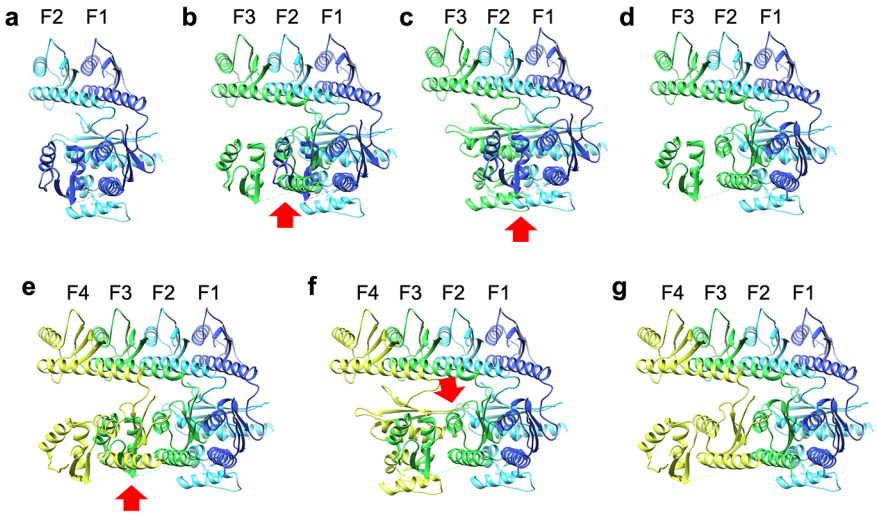


**Supplementary Fig. 11. Ribbon representation of the CCW growth model of MS-ring formation. (a)** Ribbon model of two RBM1-RBM2-RBM3 units of the initial FliF dimer (F1 in blue and F2 in cyan). **(b)** When the third subunit (F3 in green) is placed to the left of F2, serious steric hinderance occurs between RBM1 of F1 and RBM2 of F3 (shown by red arrow). **(c)** When RBM1-2 of F3 is placed in the conformation of Mol-B of the 33-mer MS-ring, steric hinderance also occurs between two RBM1-2 units of F2 and F3 (shown by red arrow). **(d)** Placement of RBM1-2 of F3 induces the dissociation of RBM1 from RBM2 in F1 to allow association of two RBM2 units of F1 and F3 to start forming the inner core RBM2-ring. **(e)** When the fourth subunit (F4 in yellow) is placed on the left side of F3, serious steric hinderance occurs between RBM1 of F3 and RBM2 of F4 (shown by red arrow). **(f)** When RBM1-2 of F4 is placed in the conformation of Mol-B, steric hinderance occurs again between two RBM1-2 units of F2 and F4 (shown by red arrow). **(g)** Placement of RBM1-2 of F4 forces RBM1 to detach from RBM2 in F3 to allow RBM2 of F4 to bind to RBM2 of F3 to grow the RBM2-ring.

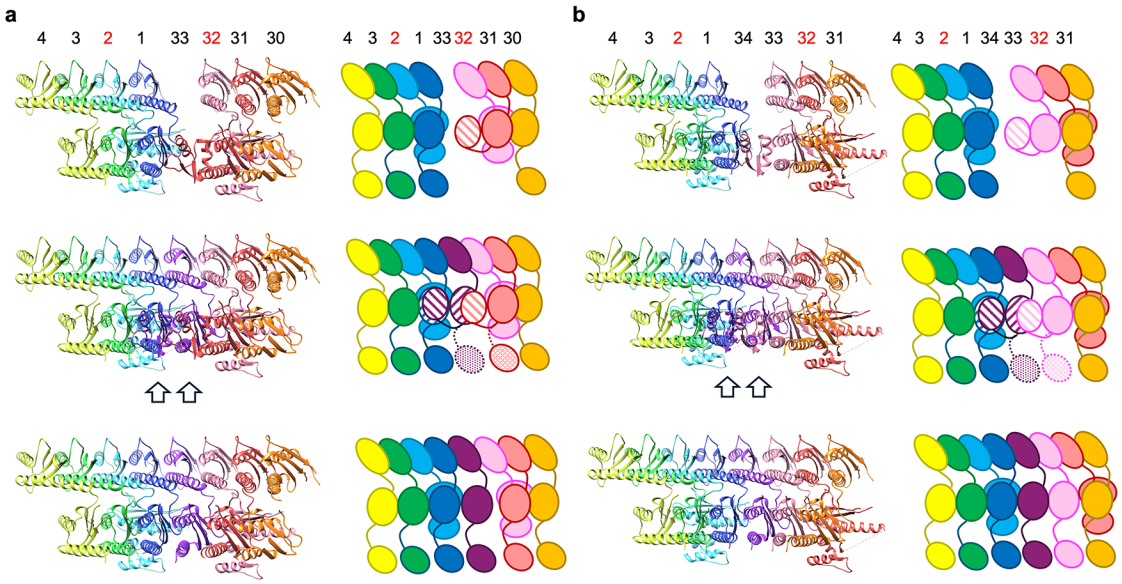


**Supplementary Fig. 12. Model for the final step of MS-ring formation. (a)** The final step of 33-mer MS-ring formation and **(b)** 34-mer MS-ring formation are shown in ribbon (left) and schematic representations (right). Top panels, before insertion of the final subunit; Middle panels, steric hindrance by the insertion of the final subunit; Bottom panels, completion of MS-ring formation. The subunit numbers are shown above each model.

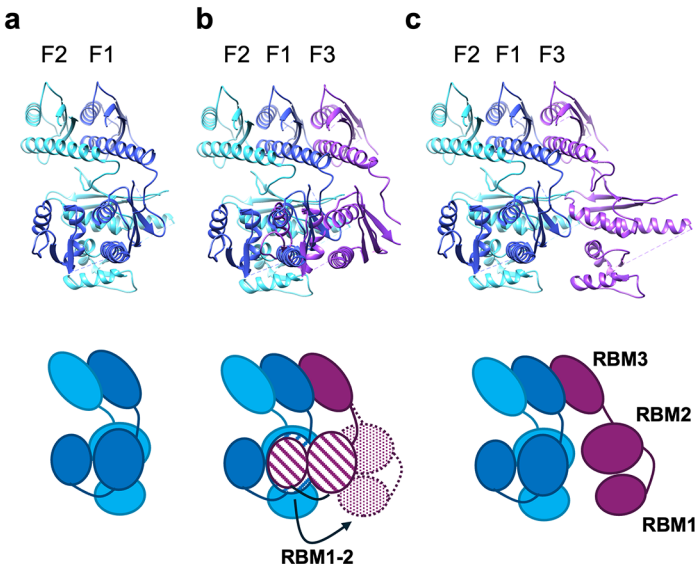


**Supplementary Fig. 13. CW growth model of MS-ring formation. (a-c)** Ribbon (top) and schematic (bottom) representations of the CW growth model. **(a)** Model for the RBM1-3 unit of the initial FliF dimer. **(b)** When the third subunit (F3) binds to the initial dimer on the right, steric hinderance occurs between RBM1 of F3 and RBM2 of F1 (shown by stripe pattern), and therefore, RBM1-2 of F3 move outward to avoid the clash but cannot be stabilized due to the lack of it binding site. **(c)** RBM1-2 of F3 moves freely, and no further ring growth occurs. Thus, MS-ring formation does not proceed in the CW direction.

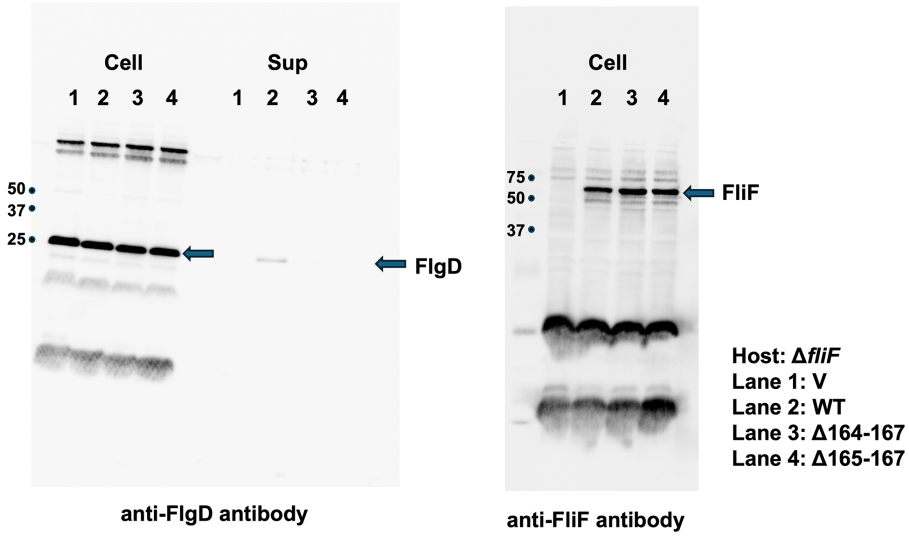


**Supplementary Fig. 14. Original immunoblots shown in Fig. 4c.** The regions of interest were indicated by arrows. The positions of molecular mass markers (kDa) are indicated on the left.

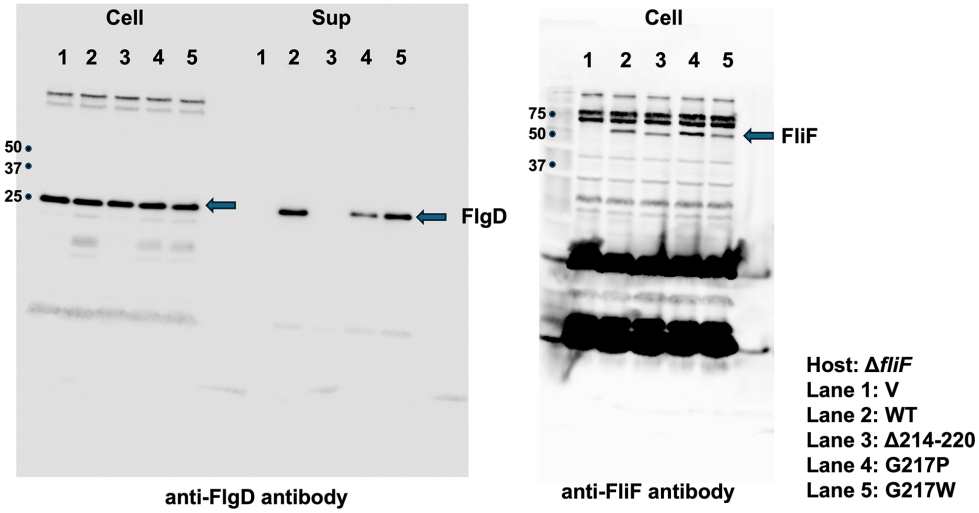


**Supplementary Fig. 15. Original immunoblots shown in Fig. 5c.** The regions of interest were indicated by arrows. The positions of molecular mass markers (kDa) are indicated on the left.

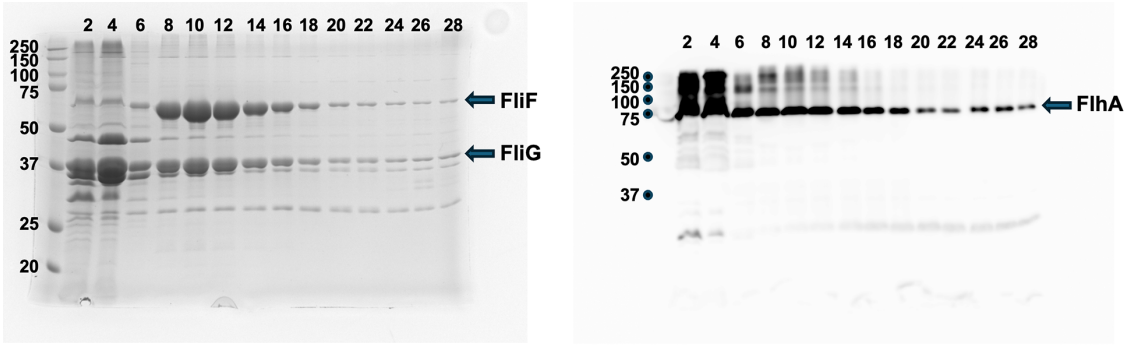


**CBB staining** **anti-FlhA antibody**

**Supplementary Fig. 16. Original CBB-staining gel and immunoblot shown in Supplementary Fig. 1a.** The regions of interest were indicated by arrows. The positions of molecular mass markers (kDa) are indicated on the left.

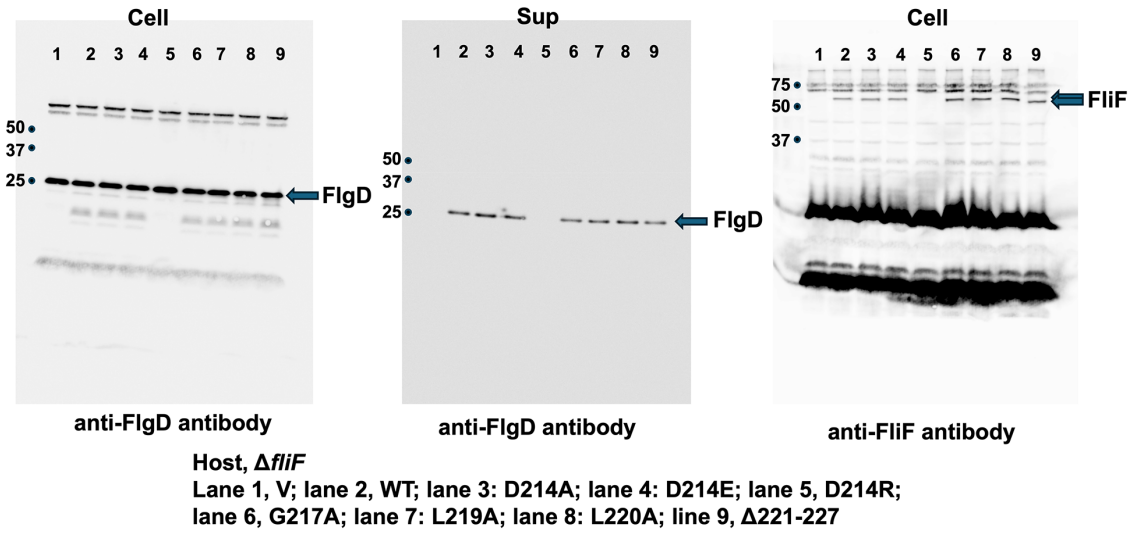


**Supplementary Fig. 17. Original immunoblots shown in Supplementary Fig. 9b.** The regions of interest were indicated by arrows. The positions of molecular mass markers (kDa) are indicated on the left.

**Supplementary Table 1. Inner diameters of the S-ring and β-collar**

| PDB ID | Inner diameter of the S-ring (Å) | Inner diameter of the β-collar (Å) |
|---|---|---|
| **C33** | | |
| 8ZDT (This study) | 141 | 101 |
| 6SD1 | 138 | 98 |
| 8FTF | 141 | 104 |
| | | |
| **C34** | | |
| 8ZDU (This study) | 146 | 105 |
| 6SD4 | 140 | 102 |
| 7D84 | 144 | 103 |
| 7NVG | 142 | 103 |

**Supplementary Table 2. Strains and plasmids used in this study**

| ***Salmonella*** **strains and Plasmids** | **Relevant characteristics** | **Source or reference** |
|---|---|---|
| *Salmonella* | | |
| SJW1368 | Δ(*cheW-flhD*); master operon mutant | 1 |
| TH12415 | Δ*fliF* | K. T. Hughes |
| | | |
| Plasmids | | |
| pET3c | Expression vector | Novagen |
| pTrc99AFF4 | Expression vector | 2 |
| pMKM20001 | pTrc99CES3/ FliO + His-FliP + HA-FliQ + FliR-FLAG + FlhA + FlhB + FliF + FliG | 3 |
| pMKMiF001 | pET3c/ FliF | 4 |
| pMKMiF002 | pET3c/ FliF(I252A) | 4 |
| pMKMiF002-SP1 | pET3c/ FliF(I252A/R228C) | This study |
| pMKMiF002-SP2 | pET3c/ FliF(A252V) | This study |
| pMKMiF015 | pTrc99AFF4/ FliF | This study |
| pMKMiF015(Δ164-167) | pTrc99AFF4/ FliF(Δ164-167) | This study |
| pMKMiF015(Δ165-167) | pTrc99AFF4/ FliF(Δ165-167) | This study |
| pMKMiF015(Δ214-220) | pTrc99AFF4/ FliF(Δ214-220) | This study |
| pMKMiF015(Δ221-227) | pTrc99AFF4/ FliF(Δ221-227) | This study |
| pMKMiF015(D214A) | pTrc99AFF4/ FliF(D214A) | This study |
| pMKMiF015(D214E) | pTrc99AFF4/ FliF(D214E) | This study |
| pMKMiF015(D214R) | pTrc99AFF4/ FliF(D214R) | This study |
| pMKMiF015(G217A) | pTrc99AFF4/ FliF(G217A) | This study |
| pMKMiF015(G217P) | pTrc99AFF4/ FliF(G217P) | This study |
| pMKMiF015(G217W) | pTrc99AFF4/ FliF(G217W) | This study |
| pMKMiF015(L219A) | pTrc99AFF4/ FliF(L219A) | This study |
| pMKMiF015(L220A) | pTrc99AFF4/ FliF(L220A) | This study |

## References


1. Ohnishi, K., Ohto, Y., Aizawa, S., Macnab, R. M. & Iino, T. FlgD is a scaffolding protein needed for flagellar hook assembly in *Salmonella typhimurium*. *J. Bacteriol.* **176**, 2272–2281 (1994).
2. Ohnishi, K., Fan, F., Schoenhals, G.J., Kihara, M. & Macnab, R.M. The FliO, FliP, FliQ, and FliR proteins of *Salmonella typhimurium*: putative components for flagellar assembly. *J. Bacteriol.* **179,** 6092–6099 (1997).
3. Takekawa, N. *et al*. Two distinct conformations in 34 FliF subunits generate three different symmetries within the flagellar MS-ring. *mBio* **12**, e03199-20 (2021).
4. Kawamoto, A. *et al*. Native flagellar MS ring is formed by 34 subunits with 23-fold and 11-fold subsymmetries. *Nat. Commun.* **12**, 4223 (2021).